Competition effects in the dynamics of tumor cords

M. Scalerandi,[1] B. Capogrosso Sansone,[1,2] C. Benati,[1] and C. A. Condat[3,4]

[1]*INFM, Dipartmento Fisica, Politecnico di Torino, 10129 Torino, Italy*
[2]*Los Alamos National Laboratory, Los Alamos, New Mexico 87545*
[3]*FaMAF, Universidad Nacional de Cordoba, Cordoba, Argentina*
[4]*Department of Physics, University of Puerto Rico, Mayaguez, Puerto Rico 00680*

A general feature of cancer growth is the cellular competition for available nutrients. This is also the case for tumor cords, neoplasms forming cylindrical structures around blood vessels. Experimental data show that, in their avascular phase, cords grow up to a limit radius of about 100 μm, reaching a quasi-steady-state characterized by a necrotized area separating the tumor from the surrounding healthy tissue. Here we use a set of rules to formulate a model that describes how the dynamics of cord growth is controlled by the competition of tumor cells among themselves and with healthy cells for the acquisition of essential nutrients. The model takes into account the mechanical effects resulting from the interaction between the multiplying cancer cells and the surrounding tissue. We explore the influence of the relevant parameters on the tumor growth and on its final state. The model is also applied to investigate cord deformation in a region containing multiple nutrient sources and to predict the further complex growth of the tumor.

I. INTRODUCTION

Competition for nutrients is a critical tumor growth determinant. Nutrients are carried through the vascular system by the blood and, after crossing the vessel walls, diffuse through the tissue until they reach the individual cells. The availability of enough nutrient is essential for cancer cell multiplication and tumor growth. In most neoplasms, the complexity of the local anatomy and the irregular vascular structure conspire to make the precise prediction of tumor evolution a very difficult task. Besides, there are number of other factors, such as angiogenic growth and the development of metastases, which seldom can be kept under control and influence the late growth stages.

Nevertheless, the initial avascular phase of solid tumor growth usually shows a certain degree of regularity. This is the case for tumor cords, which are formed by malignant cells proliferating in cylindrical structures around blood vessels [1–3]. Experimental data show that, in its avascular phase, the neoplasm grows up to a limit radius of about 60–140 μm and is always surrounded by necrotized regions [4]. This quasi-steady-state is reached because the high consumption by the proliferating cancer cells leads to a radial decay of the oxygen tension and of the concentration of other essential nutrients, such as glucose and iron. Oxygen and nutrient deprivation causes a reduction in the number of proliferating cells along the radial direction, limiting cord growth [5]. This state of affairs is usually only temporary. Cancer cells release molecular factors that stimulate the formation of a vascular network inside the tumor [6]. Due to the increased amount of nutrient available to the tumor surface, growth starts again and the tumor expands to regions distant from the central vessel. Eventually metastasis occurs.

From a physicist's perspective, the study of nutrient distribution in healthy tissue is relatively simple: the number of cells can be considered fixed and the system is in a steady state characterized by the equilibrium between the nutrient diffusion and its absorption by the tissue. The problem of oxygen diffusion in healthy tissue surrounding an isolated straight vessel was already considered by Krogh in 1919 [7]. Krogh's model has been extended to incorporate such features as oxygen-pressure-dependent consumption and multicylindrical structures. Interesting results can be obtained by using analytical methods [8]. The situation is radically different after the onset of tumor growth: cancer cell multiplication and the advance of the tumor front lead to a continuously evolving distribution of nutrient sinks and to the development of mechanical stresses. As a consequence, an adequate description becomes much harder.

Numerous mathematical models have been developed [9] to analyze tumor growth, both in its avascular [10–14] and vascular [15] phases. Kinetic models have been applied to describe the steady states of tumor cords, leading to qualitative agreement with experimental data [16,17]. We note that, because of the inherent difficulties of the problem, these models generally contain some simplifying assumptions, such as keeping a constant cell volume density or describing cell fluxes using a velocity field [16,18]. The relaxation of these assumptions would strengthen the correspondence between models and real biological processes.

By taking full advantage of the symmetries and considering a somewhat idealized situation, Bertuzzi and co-workers were able to make predictions about the growth of tumor cords using purely analytical methods [19]. Since we will not attempt an analytical solution, we will be free from the need to resort to the *a priori* mathematical assumptions introduced in previous models [13,16,19]. In fact, the proposed model will be based only on simple biological properties, conveniently described as physical processes. As such, it will lead to macroscopic predictions resulting from microscopic assumptions, while in previous models microscopic assumptions have been often formulated to accommodate to macroscopic observations (e.g., in our model the radial decay of the oxygen tension is not an *a priori* assumption, but it re-

sults from a reaction-diffusion process in which cellular evolution plays a basic role).

From the point of view of energy utilization, cells may be described as particles carrying a certain amount of stored energy that controls their transition between quiescent and proliferating states [20,21]. Following this line of thought, cells have been modeled using the concept of particles with an energy depot to describe the relation between stored energy and the motion of small microorganisms [22,23]. Tumor growth is determined by the interaction between these particles and the local environment, which is characterized by the competition for nutrients [12,24] and space [25,26].

Applying the local interaction simulation approach (LISA) [27], we have recently proposed a model [12] that includes the features described above to simulate tumor growth in tissues with an arbitrary anatomical configuration and vascularization structure [26]. This model allows us to predict the spatiotemporal evolution of neoplasms, conceived not as geometrical objects with assigned internal and boundary conditions, but rather as a grouping of identical, yet individual, cells interacting at a local level. In this approach, the model is directly implemented in terms of discrete iteration equations, which allows for its easy adaptation to different situations, in a form suitable for their computational solution using, for example, parallel processing.

The purpose of this paper is to adapt and generalize the model of Ref. [12] to describe the evolutive and quasiequilibrium stages of a tumor cord. The model will enable us to investigate the effects of real biological features, such as tumor aggressiveness, on cord growth. It will be also used to study how the tumor evolves beyond the single-cord stage when there are other nutrient sources in the neighborhood.

In the following section we present the biological motivation for our model and its implementation in terms of discrete equations. A detailed numerical study of the model solutions in the avascular phase is given in Sec. III. Section IV extends the description beyond the single-cord problem.

II. THE MODEL

Tumor cords are dynamic structures developing in a given (generally soft) environment around a blood vessel. As a result of the local nutrient availability, a (normal or neoplastic) cell may be either in a quiescent, a mitotic (proliferating), or an apoptotic (dying) phase. Since chemicals diffuse from the vessel to the periphery and are absorbed by cells, nutrient concentration decays rapidly with increasing distance from the sources. As a consequence, cancer cells closer to the vessels are the ones more likely to be in a mitotic phase. The pressure generated by these dividing cells creates a continuous outward migration. Healthy cells are normally quiescent, but they may starve at the nutrient-depleted tumor fringes. Since we will be considering pressure effects, we will also need to make assumptions about the compressibility of the various cell species, which we will label with the variable l.

Due to the symmetry of the problem, we can suitably model the above-described features by considering a two-dimensional grid with $N_x \times N_y$ elements. We denote with n_{ij}^t

the number of nutrient molecules located in element (i,j) at time t (the time will be discretized with step τ). Similarly, we call $c_{ij}^t(l)$ the number of cells of the lth species. The following cell types are considered.

Cancer cells ($l=0$), characterized by a high affinity for nutrients, which leads to fast proliferation. They are assumed to have an intermediate rigidity.

Necrotic cells ($l=1$), resulting from the apoptosis of both healthy and cancer cells. They do not take part in metabolic processes and are slowly reabsorbed. They have a large rigidity.

Healthy cells ($l=2$), which, due to their low nutrient affinity, are almost always in a quiescent state. They are considered soft tissue.

Vessel-lining *endothelial* cells ($l=3$), which define the nutrient sources and are always in a quiescent state. Since they feed directly from the bloodstream, they do not compete with other cells for nutrient acquisition. Vessels are considered perfectly rigid here, although in our approach it would be possible to model also their compression, the migration of cells across their walls, or the development of angiogenesis [28,29].

Liquid substances ($l=4$), which result from the disgregation of the necrotic cells and are pushed out of the specimen when compression increases.

Each cell is modeled as a sphere with radius r_0 (cell sizes are assumed to be the same for all species). When the available space is not sufficient, cells are compressed, their average instantaneous radius becoming r_{ij}^t. As a consequence stress appears and slowly relaxes, deforming the surrounding medium and eventually pushing cells away. Nutrient molecules, which are small compared to cells, do not occupy space.

In the following subsections, we will define the interactions (among cells and between cells and environment), which, once the initial and boundary conditions are stated, determine the system evolution.

A. Cell behavior

The state (quiescent, mitotic, or apoptotic) of cells belonging to the lth species is determined by the amount of their intracellular energy $b_{ij}^t(l)$, i.e., the energy stored in the cell in the form of binding energy of molecules.

If $b_{ij}^t(l) > Q_m(l)$, where $Q_m(l)$ is the mitosis threshold for the lth species, proliferation takes place,

$$c_{ij}^t(l) \rightarrow (1+R_m)c_{ij}^t(l),$$

where R_m is the proliferation rate. The stored energy is redistributed between parent and daughter cells and partly consumed (at a rate R_c) during the process,

$$b_{ij}^t(l) \rightarrow \frac{(1-R_c)}{(1+R_m)}b_{ij}^t(l).$$

If $b_{ij}^t(l) < Q_a(l)$, where $Q_a(l)$ is the apoptosis threshold for the lth species, some of the cells become necrotic,
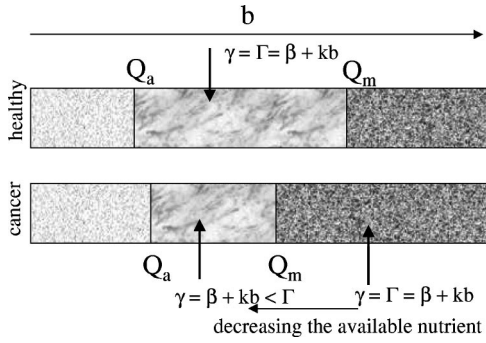
FIG. 1. Thresholds for healthy and cancer cells. The quiescence domain for healthy cells is much larger, and their energy fluxes are usually in equilibrium inside the quiescent region, with $\Gamma(2) \approx \beta(2) + kb(2)$. Cancer cells are much more labile; by decreasing the amount of available nutrient, proliferation may shift the equilibrium position from the mitotic to the quiescent state. Competition may further decrease $\Gamma(0)$, pushing cancer cells into the apoptotic stage.

$$c_{ij}^t(l) \to (1 - R_a) c_{ij}^t(l), \quad \forall l \neq 1,4,$$

$$c_{ij}^t(1) \to c_{ij}^t(1) + \sum_{l \neq 1} R_a c_{ij}^t(l) - R_r c_{ij}^t(1),$$

$$c_{ij}^t(4) \to c_{ij}^t(4) + R_r c_{ij}^t(1),$$

where R_a is the apoptosis rate. Necrosis is partly reabsorbed (e.g., by macrophages) and transformed into liquid substances; R_r is the reabsorption rate.

If $Q_a(l) < b_{ij}^t(l) < Q_m(l)$, cells are in a quiescent state.

The amount $b_{ij}^t(l)$ of stored energy per cell is determined by the balance between the per cell amounts of energy absorbed $[\gamma_{ij}^t(l)]$, released $[\delta_{ij}^t(l)]$, and consumed to perform cellular metabolic functions $[\beta_{ij}^t(l)]$,

$$b_{ij}^t(l) \to b_{ij}^t(l) + \gamma_{ij}^t(l) - \beta_{ij}^t(l) - \delta_{ij}^t(l).$$

We will consider a constant and uniform per cell consumption rate $\beta_{ij}^t(l) = \beta(l)$.

The rate of energy absorption is proportional to the concentration of available nutrient when the latter is scarce, but it must saturate when it is plentiful. We model it as

$$\gamma_{ij}^t(l) = \Gamma(l) \left[1 - \exp\left(-\frac{\Phi(l) n_{ij}^t}{\sum_{l \neq 1,4} \Gamma(l) c_{ij}^t(l)} \right) \right],$$

where $\Gamma(l)$ represents the cell affinity and $\Phi(l)$ is a normalization coefficient. The released energy is proportional to the concentration of stored nutrient, $\delta_{ij}^t(l) = k(l) b_{ij}^t(l)$. Dissipation guarantees the stability of cells under small environmental perturbations. When the nutrient available is abundant, cells are in equilibrium with $\Gamma(l) \approx \beta(l) + \delta(l)$.

Different cell types are mimicked by varying the parameters. For instance, healthy and cancer cells will usually differ in both their affinities (which are larger for cancer cells) and thresholds. In the example considered in Fig. 1, the equi-

librium position for healthy cells is well inside the quiescent state. On the contrary, cancer cells are likely to satisfy the saturated $[n_{ij}^t(l) \to \infty]$ equilibrium condition $\Gamma(0) = \beta(0) + kb(0)$ for $b(0) > Q_m(0)$. However, since proliferation occurs as soon as $b(0) > Q_m(0)$, this equilibrium condition cannot be reached. In fact, the number of neoplastic cells increases and can eventually become large enough to cause nutrient scarcity. As a consequence, the true absorption rate $\gamma(0)$ becomes smaller than $\Gamma(0)$ and the equilibrium position is likely to move into the quiescent region.

B. Environment modifications

Due to space restrictions, proliferation causes cell deformation. If r_0 is the initial (unstressed) radius of a cell, its effective radius at time t becomes

$$r_{ij}^t = r_0 \left[\frac{\sum_l c_{ij}^0(l)}{\sum_l c_{ij}^t(l)} \right]^{1/2}.$$

As a consequence, local stresses appear,

$$\sigma_{ij}^t = S_{ij}^t \frac{(r_{ij}^t)^2 - r_0^2}{r_0^2},$$

where

$$S_{ij}^t = \frac{\sum_l c_{ij}^t(l) S(l)}{\sum_l c_{ij}^t(l)}$$

is the elastic constant of the grid element [a weighted average of the elastic constants $S(l)$ of the various species present at the node].

Stressed cells relax inducing deformation of the surrounding tissue. As a consequence, some cells are pushed from a stressed element to a less stressed nearest neighbor. To describe this mechanism, we impose that the interface between two lattice elements moves in order to reach the equilibrium of stresses

$$\sigma_{ij}^{t+1} = \sigma_{nn}^{t+1},$$

where nn denotes one of the nearest neighbors (the process is performed separately in each direction, i.e., we consider equilibrium between quarters of cells). This equation allows us to calculate the area spanned by the interface,

$$A = \frac{1}{4} \frac{(r_{nn}^t)^2 S_{nn}^t - (r_{ij}^t)^2 S_{ij}^t + r_0^2 (S_{ij}^t - S_{nn}^t)}{(r_{nn}^t)^2 S_{nn}^t + (r_{ij}^t)^2 S_{ij}^t} \sum_l c_{ij}^t(l) \pi (r_{ij}^t)^2.$$

The cells $\Delta_{ij,nn}^t$ contained in this area migrate from (i,j) to nn. We obtain

$$\Delta^t_{ij,\text{nn}} = \sum_l \Delta^t_{ij,\text{nn}}(l)$$

$$= \frac{A}{\frac{1}{4}\sum_l c^t_{ij}(l)\pi(r^t_{ij})^2 + A} \frac{\sum_l c^t_{ij}(l)}{4} \theta(A),$$

where θ is the Heaviside function.

A distribution process, which takes into account the local populations of the various species within the grid element (i,j), allows us to calculate the amount of migrating cells per species $\Delta c^t_{ij}(l)$. This process is described in detail in Ref. [28]. It follows that,

$$c^t_{ij}(l) \rightarrow c^t_{ij}(l) + \sum_{\text{nn}} \Delta^t_{\text{nn},ij}(l) - \sum_{\text{nn}} \Delta^t_{ij,\text{nn}}(l),$$

where the sum is extended over the four nearest neighbors. Stored nutrient is accordingly redistributed.

C. Nutrients

Nutrients are molecules that diffuse from blood vessels into the tissue. Nutrient diffusion is described by the following equation:

$$n^t_{ij} \rightarrow n^t_{ij}(1 - 4\alpha) + \alpha \sum_{\text{nn}} n^t_{\text{nn}} + \Psi^t_{ij} - \Lambda^t_{ij},$$

where α is the diffusion coefficient, $\Psi^t_{ij} = n_0 c^t_{ij}(3)$ is the source term, and $\Lambda^t_{ij} = \sum_{l \neq 1,4} [\gamma^t_{ij}(l) - k(l)b^t_{ij}(l)]c^t_{ij}(l)$ is the amount of nutrient effectively absorbed by cells in element (i,j).

D. Initial and boundary conditions

We consider a square slab of tissue (one mm square) and discretize it as a 100×100 grid. Healthy cells are located in each grid element. A circular vessel, with radius 30 μm (in agreement with the experimental data), goes through the center $[(i,j) = (50,50)]$ of the specimen. Smaller vessels are also distributed along the specimen edge to represent nutrient flux from other sources. Tumor cells are initially distributed forming a thin cylindrical layer around the vessel. We write,

$$c^0_{ij}(0) = 100 \quad \text{for} \quad 9 < (i-50)^2 + (j-50)^2 < 10,$$

$$c^0_{ij}(3) = 100 \quad \text{for} \quad (i-50)^2 + (j-50)^2 < 9,$$

$$c^0_{ij}(3) = 90 \quad \text{for} \quad (i=1,100,\forall j),(j=1,100,\forall i),$$

$$c^0_{ij}(2) = 100 \quad \text{elsewhere},$$

$$c^0_{ij}(1) = 0 \quad \text{everywhere}.$$

The initial nutrient distribution corresponds to the stationary condition in the absence of cancer cells and is calculated using the same code without neoplastic cells.

TABLE I. List of the parameters used for the various cases.

		Cancer cells	Healthy cells
Γ	Affinity		0.027
β	Consumption		0.017
k	Desorption	0.01	0.01
S	Elastic constant	10	1
Q_m	Mitosis threshold	0.6	2.0
R_m	Mitosis rate	0.1	0.1
Q_a	Apoptosis threshold	0.1	0.1
R_a	Apoptosis rate	0.1	0.1

Boundary conditions are rigid, due to the presence of vessels along the borders. Most of the dynamics develops in the central part of the specimen anyway, so boundaries hardly affect the tumor evolution.

III. CORD DYNAMICS-PARAMETER ANALYSIS

The proposed model allows us to study the influence of the various parameters on the dynamics of tumor cords. In this section we will analyze the case of a neoplasm growing around a single vessel. We will compare the model predictions with available experimental data, which show that in the avascular phase the tumor grows up to a limit radius of about 60–140 μm according to its malignancy and the oxygen tension profile [4]. The parameters chosen for the simulations are reported in Table I. In addition we have $\alpha = 0.2$, $n_0 = 2000$, $R_r = 0.05$. Because no confusion can arise, in the following we call $\beta(0) = \beta$ and $\Gamma(0) = \Gamma$.

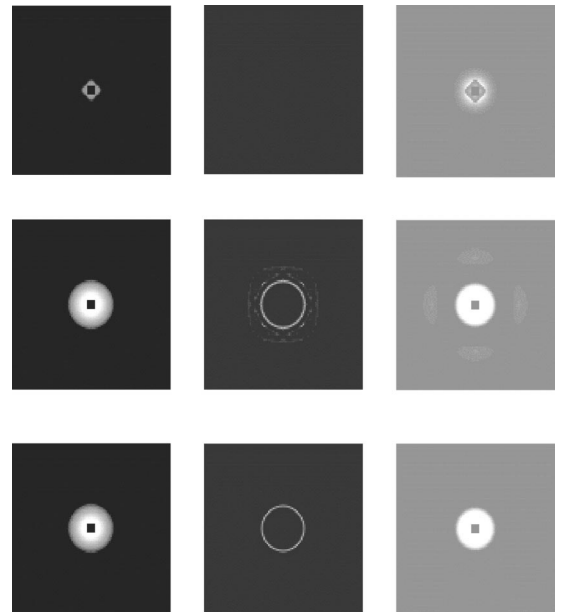In Fig. 2 we present snapshots taken at successive times

FIG. 2. Snapshots of the cancer cell, necrotized cell, and stress distributions, reported in the left, central, and right columns, respectively. The corresponding times are indicated at the left. Here $\Gamma = 0.03$ and $\beta = 0.01$.
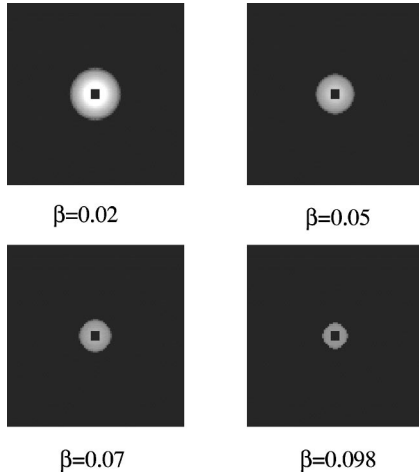
FIG. 3. Snapshots of the quasistatic cell distributions for the specified values of the cancer cell metabolic consumption rate β. In all cases, $\Gamma - \beta = 0.01$.

FIG. 4. Number of cancer cells vs time for various values of the aggressiveness $\Gamma - \beta$. Here $\beta = 0.01$. For a very aggressive tumor cell species, the tumor mass goes through a large intermediate-time maximum. In all cases, a situation of dynamic equilibrium is reached at long times.

($t = 1000$, 1800, and 4000 arbitrary units, from top to bottom) to illustrate the system dynamics in the case of a neoplasm with $\Gamma = 0.03$ and $\beta = 0.01$. The distributions of cancer cells, necrotic cells, and stresses are reported in the left, central, and right columns, respectively. A cylindrical tumor grows around the vessel (black square at the center of the left column plots). After an initial period of slow growth (up to $t \approx 1000$), saturation is rapidly reached. There is a large concentration of cancer cells in the proximity of the nutrient source, due to fast local proliferation. The necrotic region is very thin, since dead cells are rapidly reabsorbed by macrophages, and it is almost completely localized in a circular area at the tumor front. Necrotic cells result mostly from the apoptosis of neoplastic cells, even though a few healthy cells are also involved in the apoptotic process because of the nutrient depletion induced by the tumor. These necrotic cells are visible as a tenuous ring in the $t = 1800$ snapshot. The stress distribution, shown in the third column of Fig. 2, is directly proportional to the cell deformations originating in space restrictions. As expected, larger stresses are present where proliferation is faster. The stress also propagates to regions farther from the vessel, inducing local deformations away from the tumor. Although the stress appears to be uniform in the region occupied by cancer cells, this is an effect of the scale used and we will later see that the stress intensity decays from the center towards the tumor edges. In particular, we notice that, at $t = 1800$, almost no stress is present at the interface between tumor and healthy cells, where apoptotic processes are most frequent. In fact, necrosis reabsorption induces recovery from deformation, since the disappearance of dead cells, transformed into "soft liquid" releases free space for the remaining cells. Stress relaxation is slow, but a quasi-steady-state is finally reached, with stress localized where neoplastic cells are ($t = 4000$).

The final system configuration strongly depends on the amount of energy required by the cell to perform its metabolic functions, as shown in Fig. 3, where the final distribution of neoplastic cells is reported for the values the parameter β specified in the plot ($\Gamma - \beta = 0.01$ in all four cases).
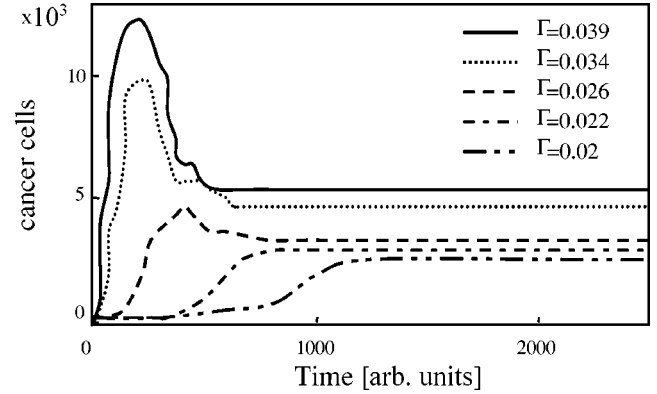
The cord radius varies between 70 and 130 μm, in agreement with the experimental data [4]. The tumor size decreases with increasing β and Γ, i.e., with increasing the intercell competition for nutrient acquisition. Due to the increase in Γ the vessel is capable of properly feeding only a smaller number of cells, nutrient scarcity becoming effective at shorter distances from the source.

The *aggressiveness* of a given cancer cell species can be defined through the reproduction speed of its members. Aggressiveness is controlled by the net energy accumulation rate $\Gamma - \beta$, which we can then take to be an indicator. We next analyze the effects of varying this indicator on the evolution of the tumor size. The number of cancer cells vs time is reported in Fig. 4 for several values of Γ (β being kept fixed). We observe that the tumor size may evolve following two different patterns.

(1) For smaller values of Γ, growth is slow during the initial stages and then it speeds up until it reaches a state of dynamic equilibrium. The necrotic region is strictly at the tumor front, which exhibits a mixture of healthy, cancer, and necrotic cells [see Fig. 5(a)].

(2) For very aggressive tumors, i.e., for large values of Γ, after a fast growth phase, apoptosis starts taking its toll, since the large number of tumor cells causes a noticeable nutrient depletion in the tissue. With the effects of nutrient scarcity being delayed with respect to the growth phase and important only at the tumor front, the tumor mass reaches a maximum and then begins to decrease. Profiles of the cell concentrations [see Fig. 5(b)] indicate the emergence of a necrotic region inside the tumor mass and, in the neighborhood of the tumor edge, of a region where cancer and healthy cells coexist.

In all cases, the system reaches an asymptotic state of dynamical equilibrium between mitosis and apoptosis, the final tumor mass increasing with Γ.

The concentration profiles are presented in Fig. 5 as functions of the distance from the vessel. At $t = 1000$ and $t = 1600$ we observe the growing neoplasm pushing outwards the surrounding healthy cells, with an increase in the total cell concentration in the region near the tumor edge. Cell
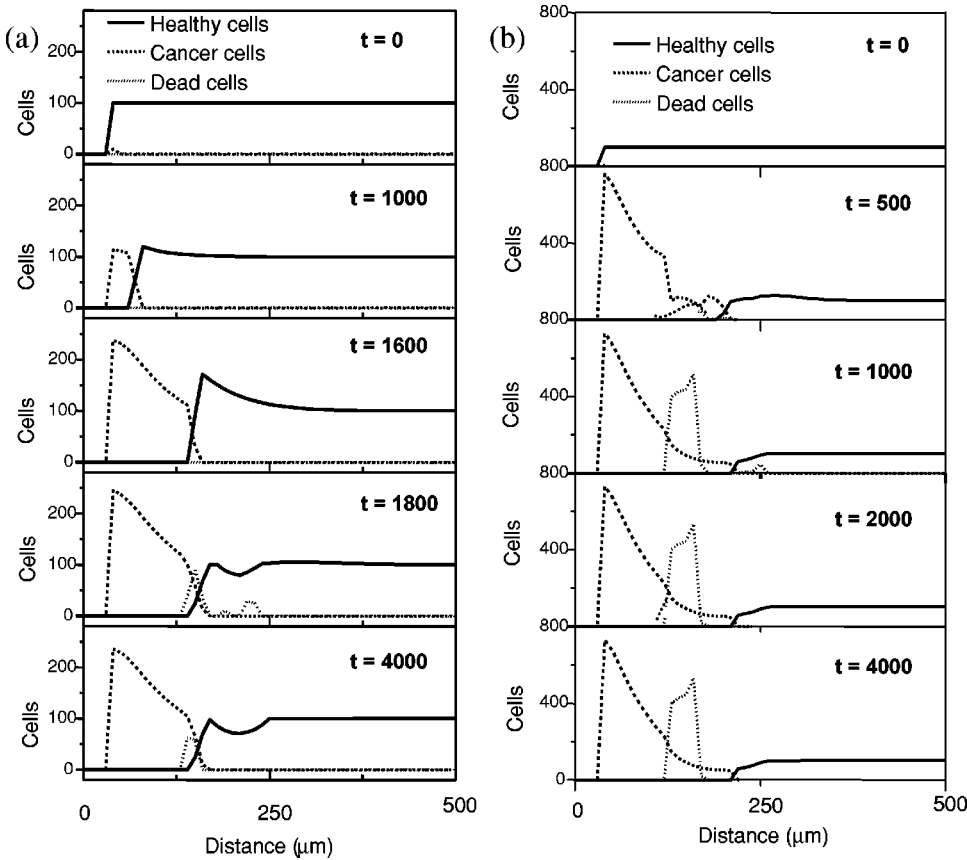
FIG. 5. Concentration profiles for healthy, cancer, and dead cells at the indicated times. (a) (b) See text, but note the emergence of a mixed tumor-necrotic region in (b).

concentration increases markedly in the neoplastic region since the release of stress is not fast enough to compensate for cell proliferation. Cells will be compressed there, but no noticeable effects will be present away from the neoplasm. Necrosis appears only at late times ($t \gtrsim 1800$) in the region where the nutrient distribution reaches a minimum. Both healthy and cancer cells start starving (see the two rather separated regions of necrosis formation at $t = 1800$). At later times, healthy cells reach a new equilibrium condition and the corresponding necrotized ring is completely reabsorbed. A slight reduction in cell density is observed at a distance $r \approx 200$ μm, where some room is occupied by the soft matter resulting from the necrosis reabsorption. The necrotic region generated by the apoptosis of cancer cells becomes stable, since continuously proliferating cells in the neoplasm core push out new necrotic cells that replace reabsorbed ones. In Fig. 5(b) we see the evolution of the profiles for a larger value of Γ. Intriguingly, a mixed tumor-necrotic region is surrounded by volumes filled purely by cancer cells.

The presence of the neoplasm causes a strong distortion in the distribution of nutrient within the tissue. In Fig. 6(a) we plot the changes in the nutrient concentration profile along the distance from the vessel with respect to the initial conditions ($n_{i,jmax/2}^t - n_{i,jmax/2}^0$) for the indicated times and the same parameter values as in Fig. 2. Of course, no changes are registered at the vessel location ($r < 30$ μm). Nutrient depletion increases while the tumor grows, but it stabilizes as the dynamic equilibrium is reached. The depletion affects even regions far from the tumor, but it is stronger in the proximity of the tumor front. The actual nutrient concentra-

tion is plotted in Fig. 6(b), where the initial concentration decrease is almost exponential, in agreement with the experimental data.

The radial stress distribution is plotted in Fig. 7. There we see that at $t = 0$ the stress is nonzero in the region where the initial tumor cells are located. At first the stress grows slowly
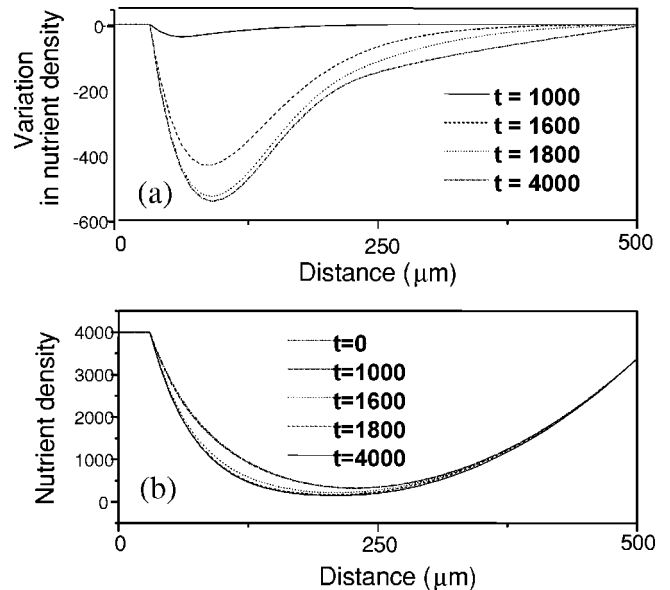

FIG. 6. (a) Relative variation and (b) absolute value of the nutrient concentration as a function of distance from the vessel axis at the indicated times.
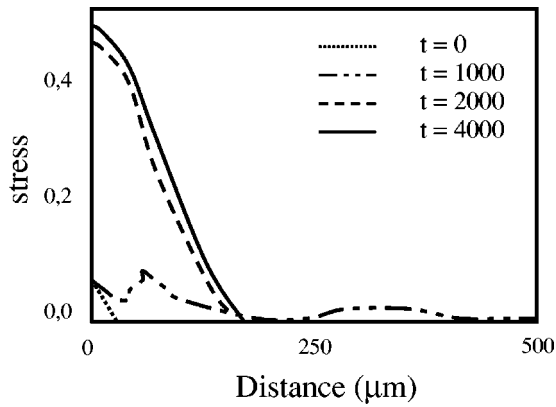
FIG. 7. Stress distribution as a function of the distance from the vessel axis at the indicated times.

(see the $t=1000$ curve), but then it becomes very large, especially in the region near the vessel, where most of the proliferation occurs. We remark that at $t=2000$ the stress disappears at $r\gtrsim 200$ μm, but it reappears far from the cord (at $r\gtrsim 300$ μm). The reason for the stress disappearance in the intervening region can be understood by looking at Fig. 5(a): in this region some of the healthy cells undergo necro-

sis, which is then reabsorbed, leaving free space and relaxing stresses. At later times, the stress in the region away from the tumor is slowly relaxed. In the region, close to the vessel, the stress reaches a stationary condition, with a maximum in the proliferation region next to the vessel wall. In this region, the confined geometry makes stress relaxation more difficult.

The volume of the neoplasm is strongly correlated to the tumor intrinsic aggressiveness and to the availability of nutrient in the surrounding environment. Another important determinant of tumoral size is the amount of energy β consumed to perform cellular metabolic (but nonproliferative) functions. The importance of this parameter is shown in Fig. 8, where the dependence of various quantities of interest on β is depicted for several values of the aggressiveness $\Gamma-\beta$. For the reasons discussed above, by increasing β the tumor mass decreases considerably (by increasing β we make competition stronger; the sources are then less capable of sustaining growth at long distances). From the resulting values for the tumor volume V we can estimate the cord radius, $r=(V/\pi)^{1/2}$, which is in agreement with observational data (50 μm$<r<130$ μm). The curves represented in Figs. 8(a), 8(b), and 8(c) can be fit very well with a sum of two exponentials. The nutrient increase, which is roughly linear, is due to the reduction in the number of cancer cells.
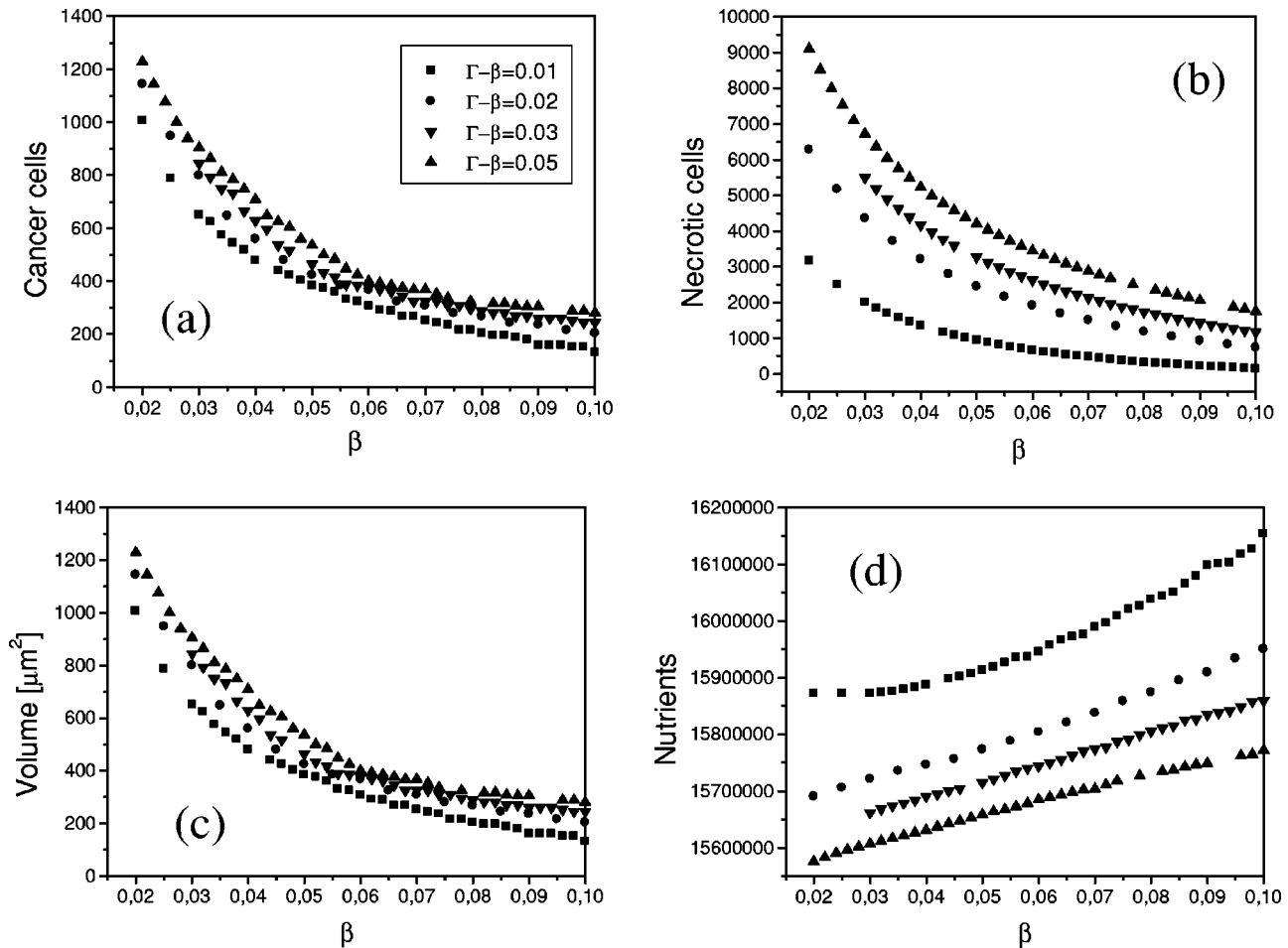

FIG. 8. Quasi-steady-state values of (a) cancer cell number, (b) dead cells number, (c) tumor volume, and (d) nutrient concentration as functions of the rate β of energy consumption for several values of the aggressiveness $\Gamma-\beta$.
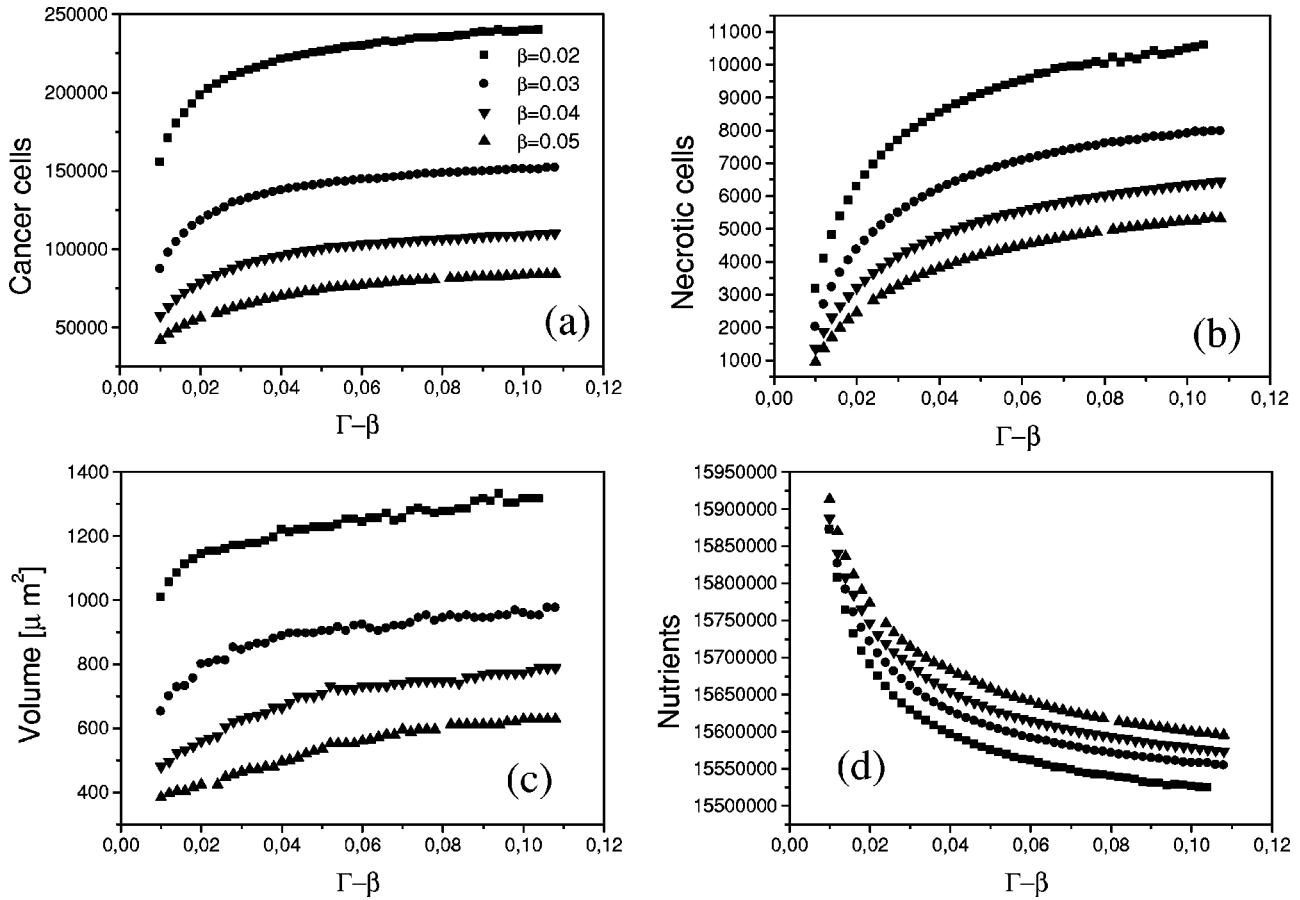
FIG. 9. Quasi-steady-state values of (a) cancer cell number, (b) dead cells number, (c) tumor volume, and (d) nutrient concentration as functions of the aggressiveness $\Gamma - \beta$ for several values of the rate of energy consumption β.

The same quantities are represented in Fig. 9, where the abscissa is the aggressiveness $\Gamma - \beta$. The number of cancer and necrotic cells, as well as the total volume are increasing functions of the malignancy for every value of β. The increase in the number of cancer cells is described by a logarithmic function.

IV. CORD EVOLUTION INTO A COMPLEX NEOPLASM

Next we consider the evolution of a neoplasm in a soft tissue containing several capillaries. We assume that the tumor originates next to a single capillary; its initial evolution is then well described in the "single capillary approximation," but, as the cord expands, cancer cells begin to sense the nutrient concentration gradients due to the presence of neighboring vessels. These favorable gradients facilitate cancer cell reproduction and the ensuing directional tumor growth towards neighboring capillaries. An instance of this behavior is shown in Fig. 10, where we report snapshots of the cancer cell concentration at different times. We observe that the neoplasm initially grows symmetrically about the capillary, some deformation being already noticed at $t = 5000$. Growth then speeds up towards neighboring capillaries and finally attains a quasi-stationary-state—other capillaries are too far and their influence is not noticed during the time scale of the simulation (the location of these capil-
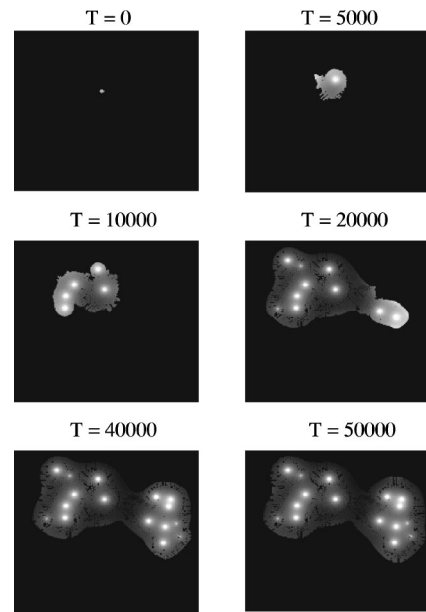

FIG. 10. Evolution of a neoplasm in a multicapillary environment. At $t = 5000$, the initial cord has begun to deform, branching off towards neighboring capillaries. After a stage of rapid growth a quasi-steady-state is reached. Other vessels are too far to influence the tumor development in preangiogenic stages.

Neoplastic cells   Necrotic cells
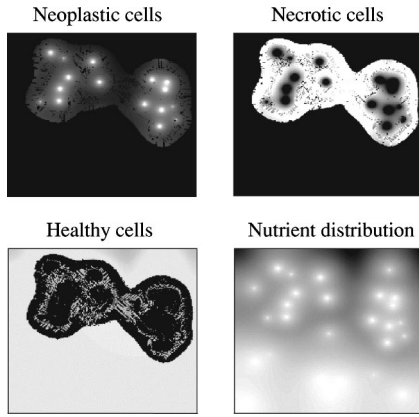
Healthy cells   Nutrient distribution

FIG. 11. Cell and nutrient concentrations for the quasi-steady-state of the tumor whose evolution is depicted in Fig. 10. Note in particular the rapid decay of nutrient concentration near the cancer-surrounded capillaries. A much gentler decay is observed about the cancer-free capillaries at the bottom of the figure.

laries is visible in the last snapshot of Fig. 11). This can be verified by linear plots of the total cancer and necrotic cell numbers as functions of time, which flatten out after $t \approx 40\,000$. It is likely that, under the reported conditions, the tumor will further expand through the angiogenic process.

If we neglect angiogenesis, the final configurations of cells and nutrients corresponding to the neoplasm of Fig. 10 are those reported in Fig. 11. The tumor contains large necrotized regions corresponding to areas where the nutrient depletion caused generalized cancer cell death. Of course, there is no necrosis in the immediate neighborhood of the vessels. Inside the tumor, small islands of healthy cells survive in the periphery of the regions with high cancer cell concentrations. Note the marked healthy cell depletion in the neighborhood of the highly necrotized tumor rim. Since cancer cells behave as strong sinks, the nutrient distribution decreases very fast as we move away from the capillaries. The contrast with the much slower variation in the nutrient concentration in the neighborhood of the cancer-free vessels (visible at the bottom of the nutrient distribution graph) is evident. These results are qualitatively what we would expect for tumoral growth in soft tissues, such as brain [30].

V. CONCLUSION

In this paper we have presented a nutrient competition model that describes the growth of tumor cords. By introducing simple assumptions at the cellular level, the model can predict the main cord features during its growth and quasi-steady-state stages. The model permits the direct evaluation of the influence of realistic parameters such as the aggressiveness and the rate of nutrient consumption by cancer cells. Nonhomogeneous and anisotropic environments can be also easily incorporated. In all cases the cord evolves to a final stage where an inner core of cancer cells surrounds

the vessel and is surrounded by a necrotized shell. In this quasi-steady-state individual cancer cells will die and be replaced by newly formed cells, whereas necrotic cells are slowly disgregated.

It was predicted in Ref. [19] that necrosis might occur *within* the tumor tissue, in such a way that a necrotized shell would separate an inner cylinder formed by tumor cells from an outer annulus also formed by tumor cells. Although we never observed this situation, Fig. 5(b) describes the emergence of an annular mixed region where cancer and dead cells coexist, surrounded by domains of purely cancerous tissue. This occurs for high values of the uptake rate Γ. We believe that at the inner edge of the mixed region the cell concentration is too high to permit the survival of all cancer cells. Apoptosis ensues for some of them, but those that get far enough may reach a region, which, although depleted of nutrients, can support a relatively small concentration of cancer cells. It is conceivable that, under some special conditions, cancer cells could have reached initially regions relatively remote from the vessel and then, although cut off from the central tumor by a completely necrotized layer, they are able to survive precisely because that layer lets through enough nutrient.

We also considered the evolution of a tumor cord in the presence of neighboring vessels. Due to the nutrient concentration gradient, the growing tumor loses its cylindrical symmetry and starts growing towards neighboring vessels. If there are no vessels in the immediate neighborhood, the tumor growth will be arrested. Eventually fast growth would be rekindled by the onset of angiogenesis. In this paper we have considered only preangiogenic stages, so that nutrient sources are fixed. However, the transition to a vascular phase [31,29] must be included if we want to predict the *in vivo* evolution of the tumor at all times. Since the vascular structure is already explicitly incorporated into our model, the extension to describe the angiogenic phase is possible without modifications in the basic features of the model. This extension and possible therapeutical applications of the model presented here will be discussed elsewhere.

If the experimental values for some relevant cell processes were available (e.g., nutrient intake and consumption rates and cell growth rates under pressure), we could have already a quantitatively reliable description of the dynamics of cord growth, connecting microscopic data to macroscopic phenomenology. However, we have not been able to find a consistent set of cellular data that could be used as input for our simulations. One of the purposes of this paper is to help to motivate experiments in this direction.

[1] J. V. Moore, H. A. Hopkins, and W. B. Looney, Radiat. Environ. Biophys. **23**, 213 (1984).

[2] J. V. Moore, P. S. Hasleton, and C. H. Buckley, Br. J. Cancer **51**, 407 (1985).

[3] K. H. Falkvoll, Acta Oncol. **29**, 935 (1990).

[4] J. V. Moore, H. A. Hopkins, and W. B. Looney, Eur. J. Cancer Clin. Oncol. **19**, 73 (1984).

[5] D. G. Hirst, J. Denekamp, and B. Hobson, Cell Tissue Kinet. **15**, 251 (1982); D. G. Hirst, V. K. Hirst, B. Joiner, V. Prise, and K. M. Shaffi, Br. J. Cancer **64**, 54 (1991).

[6] J. Folkman, Adv. Cancer Res. **43**, 175 (1985).

[7] A. Krogh, J. Physiol. (London) **52**, 409 (1919).

[8] L. Hoofd, in *Oxygen Transport in Biological Systems*, edited by S. Eggington and H. F. Ross (Cambridge U. Press, Cambridge, 1992).

[9] *A Survey of Models for Tumor-Immune System Dynamics*, edited by J. A. Adam and N. Bellomo (Birkhäuser, Boston, 1997).

[10] A. Brù, J. M. Pastor, I. Fernaud, I. Brù, S. Melle, and C. Berenguer, Phys. Rev. Lett. **81**, 4008 (1998).

[11] S. C. Ferreira, M. L. Martins, and M. J. Vilela, Physica A **272**, 245 (1999).

[12] M. Scalerandi, A. Romano, G. P. Pescarmona, P. P. Delsanto, and C. A. Condat, Phys. Rev. E **59**, 2206 (1999); P. P. Delsanto, A. Romano, M. Scalerandi, and G. P. Pescarmona, *ibid.* **62**, 2547 (2000).

[13] H. M. Byrne, J. Math. Biol. **39**, 59 (1999).

[14] M. A. J. Chaplain, D. L. Benson, and P. K. Maini, Math. Biosci. **121**, 1 (1994).

[15] E. Stott, N. F. Britton, J. A. Glazier, and M. Zajac, Math. Comput. Modell. **30**, 183 (1999).

[16] A. Bertuzzi and A. Gandolfi, J. Theor. Biol. **204**, 587 (2000).

[17] D. L. S. McElwain and G. J. Pettet, Bull. Math. Biol. **55**, 655 (1993).

[18] J. A. Adam and S. A. Maggelakis, Bull. Math. Biol. **52**, 549 (1990).

[19] A. Bertuzzi, A. Fasano, and A. Gandolfi, in *Free Boundary Problems: Theory and Applications*, edited by N. Kenmochi (Gakkotosho, Tokyo, 2000), Vol. II.

[20] T. Hofer, J. A. Sherratt, and P. K. Maini, Physica D **85**, 425 (1995).

[21] J. C. M. Mombach and J. Glazier, Phys. Rev. Lett. **76**, 3032 (1996).

[22] F. Schweitzer, W. Ebeling, and B. Tilch, Phys. Rev. Lett. **80**, 5044 (1998).

[23] C. A. Condat and G. J. Sibona, Physica A (to be published).

[24] R. Halvosrud and G. Wagner, Phys. Rev. E **57**, 941 (1998).

[25] A. J. Perumpanani *et al.*, Physica D **126**, 145 (1999).

[26] B. Capogrosso Sansone, P. P. Delsanto, M. Magnano, and M. Scalerandi, Phys. Rev. E **64**, 021903 (2001).

[27] P. P. Delsanto *et al.*, Science **265**, 1188 (1994); P. P. Delsanto *et al.*, in *New Perspectives on Problems in Classical and Quantum Physics*, edited by P. P. Delsanto and A. W. Saenz (Gordon and Breach, New Delhi, 1998), Vol. 2, p. 51.

[28] M. Scalerandi, B. Capogrosso Sansone and C. Camagna, Phys. Rev. E (to be published).

[29] B. Capogrosso Sansone, M. Scalerandi, and C. A. Condat, Phys. Rev. Lett. **87**, 128102 (2001); M. Scalerandi, B. Capogrosso, and C. A. Condat, Phys. Rev. E **65**, 011902 (2002); M. Scalerandi, G. P. Pescarmona, P. P. Delsanto, and B. Capogrosso Sansone, Phys. Rev. E **63**, 011901 (2000).

[30] Y. Yoshii, K. Narushima, K. Tsuboi, Y. Maki, and K. Sugiyama, J. Neuro-Oncol. **6**, 119 (1988).

[31] M. J. Holmes and B. D. Sleeman, J. Theor. Biol. **202**, 95 (2000).